Residual Stress Analysis of Additively Manufactured AlSi10Mg Alloy

Jiří Čapek[1,a], Karel Trojan[1,b], Radim Halama[2,c], Nikolaj Ganev[1,d], Jiří Hajnyš[2,e], Michal Kořínek[2,f] and Kamil Kolařík[1,g]

[1]*Czech Technical University in Prague; Trojanova 13, 120 00 Prague, Czech Republic;*
[2]*VSB - Technical University of Ostrava; 17. listopadu 2172/15, 708 00 Ostrava - Poruba, Czech Republic;*

[a]*jiri.capek@fjfi.cvut.cz,* [b]*karel.trojan@fjfi.cvut.cz,* [c]*radim.halama@vsb.cz,* [d]*nikolaj.ganev@fjfi.cvut.cz,* [e]*jiri.hajnys@vsb.cz,* [f]*michal.korinek@vsb.cz,* [g]*kamil.kolarik@fjfi.cvut.cz*

Abstract: The paper deals with the residual stress analysis of additively manufactured AlSi10Mg alloy. The influence of the printing strategy of SLM technology was found. The inhomogeneities of the residual stresses around the circumference of the test sample were analysed, moreover; only the tensile residual stresses were determined on the surface of as-built samples. Zones of steep changes in residual stresses (mainly tensile) can be a potential area for crack initialisation. Inherent anisotropy was studied by tracking the yield surface, from these the yield strength of 160 MPa was determined, moreover; the decrease in tensile residual stresses was estimated.

Keywords: Additive manufacturing; X-ray diffraction; Residual stresses; AlSi10Mg alloy; Inherent anisotropy

1 Introduction

Additive Manufacturing (AM), precisely Selective Laser Melting (SLM) technology, is a promising metal powder consolidation method and offers outstanding parts production opportunities. It is based on selectively melting parts of a thin flat powder bed in layers using a scanning energy source to produce 3D parts. The intricacy of the SLM process results in the magnitude and orientation of residual stresses (RS) being highly dependent on laser power, scanning speed, scanning strategy, and other processing parameters [1].

The effect of RS manifests itself in different ways. In particular, high tensile RS can lead to deformation and subsequent cracks in printed parts, which can disrupt the overall strength of the part. They can also affect the geometry of the printed object. Some shapes and structures are more sensitive to RS than others, especially in the horizontal printing strategy. Generally, tensile RS in the sub/surface layer reduce mechanical as well as corrosion properties. Furthermore, the notch toughness, fatigue resistance, and wear resistance properties are reduced; moreover, such factors as crack propagation rate, corrosion cracking, and intergranular corrosion are accelerated.

The initiation of fatigue cracks and their propagation play a significant role in fatigue properties with a strong dependence on surface roughness, microstructure parameters (dislocation density, crystallite size, microstrains), and RS [2]. In the study [3], the explicit correlation between the initialisation of surface fatigue cracks and its propagation with RS has been investigated using X-ray diffraction. It was found that not only RS but also the distribution of microstructure parameters play a crucial role in fatigue. In a previous study [4], a correlation was observed between the relaxation of structure-sensitive characteristics and the formation of surface fatigue cracks for welded materials. The basis of this

investigation will be applied to this research, which deals with the study of additively manufactured AlSi10Mg.

2 Materials and methods

For the fabrication of AlSi10Mg, for chemical composition see Table 1, tubular samples with 12.5 mm outer diameter and 10 mm inner diameter from a recycled powder Renishaw AM400 machine was used with the printing parameters shown in Table 2. During fabrication, the chamber was filled with argon with purity 5.0 to prevent oxidation and the building platform was preheated to a temperature of 170 °C. Five samples were prepared according to the printing strategy (slope related to the Z axis); 0°, 10°, 20°, 30°, and 40°. No mechanical or heat treatment was done on the printed samples to maintain a fine-grained microstructure from SLM technology, therefore; as-built samples were analysed.

Table 1. Chemical composition of AlSi10Mg alloy.

Element	Composition [wt.%]
Si	9.0–11.0
Mg	0.20–0.45
Fe	≤0.55
Cu, Mn, Zn, Ni, Pn, Sn	each ≤0.1
Ti	≤0.15
Al	Bal.

Table 2. Printing parameters.

Parameter	
Laser power	350 W
Spot size	80 μm
Layer thickness	30 μm
Printing strategy	Meander
Laser speed	1150 mm/s

Macroscopic residual stresses (RS) were determined using an Empyrean diffractometer by X-ray diffraction (XRD) when the *{311}* diffraction line of the aluminium phase was measured using chromium radiation in the direction parallel to the rotation axis of the sample (axial direction). The diffraction angles $2\theta^{hkl}$ were determined from the diffraction lines $K\alpha_1$ of the planes *{311}* of Al phase. Diffraction lines $K\alpha_1$ were fitted using the *Pearson VII* function and Rachinger's method was used for the separation of the diffraction lines $K\alpha_1$ and $K\alpha_2$. For RS determination, the $\sin^2\psi$ method and X-ray elastic constants $½s_2 = 19.05$ TPa^{-1} and $s_1 = -4.89$ TPa^{-1} were used. The experimental errors given for each value are the standard deviations of the calculation of the RS [5]. The irradiated volume was defined by the experiment geometry, the effective penetration depth of the X-ray radiation (approx. 6–11 and 5–20 μm), and the pinhole size (1×0.5 and 3×0.5 mm^2) for chromium and cobalt radiation, respectively.

The tracking of the yield surface is a semi-destructive and online method of determining the specific yield stress. Using this method, we can determine the extent of the elastic region under any combination of tensile and torsional loads on a single sample [6]. This method is based on the deviation from linearity in the form of the effective increase in plastic deformation, which is given by Eq. (1)

$$\Delta\varepsilon_{eff} = \sqrt{\Delta\varepsilon_{pl}^2 + \frac{1}{3}\Delta\gamma_{pl}^2}, \tag{1}$$

where $\Delta\varepsilon_{pl}$ and $\Delta\gamma_{pl}$ are increments of plastic deformation in the axial and torsional directions. The plasticity criterion is met as soon as $\Delta\varepsilon_{eff}$ reaches the prescribed value, which was 50 με in the following experiments. A total of 16 combinations of loading paths were used to determine the elastic area, as in [7]. Thin-walled samples with geometry for low-

cycle fatigue [8] are used for these tests. The testing equipment for the tracking tests was the LabControl biaxial hydraulic machine with a maximum load of 100 kN/1000 Nm, and the test was stress controlled at a constant rate of 1 MPa/s. The sample that was tilted by 40° from the vertical axis during printing was tracked. Tracking was repeated a total of three times to ensure statistical significance.

3 Results and discussions

Using the X-ray diffraction phase analysis, three phases were identified in the irradiated volume: approx. 85 wt.% of Al, 15 wt.% of Si, and 0.1 wt.% of intermetallic phase Mg_2Si (according to Rietveld refinement method). It is necessary to mention that, according to the chemical composition, the microstructure should be hypoeutectic, i.e., α(Al)+Si+Mg_2Si, in other words: solid solution of Al, eutectic Al+Si, and intermetallic Mg_2Si. The average crystallite size of Al and Si is 122 and 16 nm, respectively, which correlates with the fact that the matrix is coarser-grained and eutectic fine-grained in hypoeutectic alloy. Moreover, the results from Al phase are influenced by both Al, in solid solution and eutectoid too.

3.1 Residual stresses around the circumference

The distribution of the RS (Al phase) was analysed around the outer circumference of the tubular in the axial direction; see Figs. 1–2. The 0° position within the circumference was pointing down to the building platform, i.e. the printing supports side.

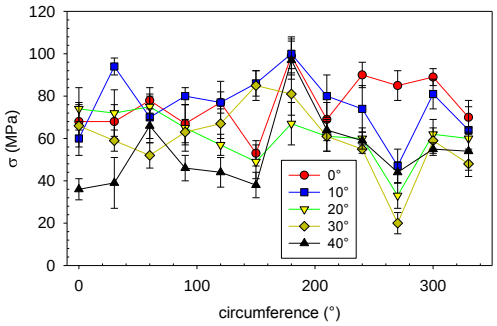

Fig. 1 Distribution of residual stresses around the circumference depending on the printing slope (related to Z axis).

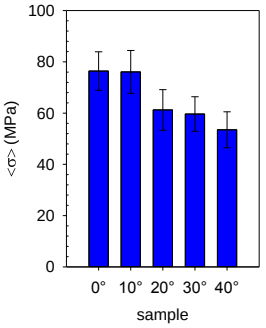

Fig. 2 Average residual stresses around the sample circumference depending on the printing slope.

The circuit distribution of RS of Al phase of all samples is inhomogeneous, moreover; all RS are tensile; see Fig. 1. The RS maxima were systematically detected at 180°, which is opposite to the printing support side. On the other hand, the minima of tensile RS were found at 270°. This effect is clearly related to the printing strategy, i.e., the inclination of the sample axis to the building platform. According to Fig. 2, the average RS around the sample circumference have a decreasing character with increasing printing slope. However, samples with higher slope have higher inhomogeneities around the sample circumference.

The circuit inhomogeneities should have a negative influence on the mechanical properties such as fatigue life, where significant changes in RS create so-called surface microstructure notches which are areas prone to the formation and propagation of fatigue cracks.

3.2 Tracking of the yield surface

The size of the elastic region is shown in Fig. 3. The effect of tracking on the distribution of RS is depicted in Fig. 4.

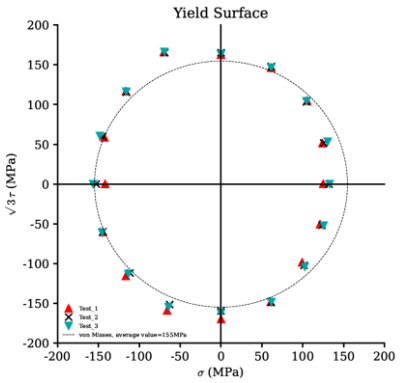

Fig. 3 The size of the elastic region for the sample printed with slope of 40°.

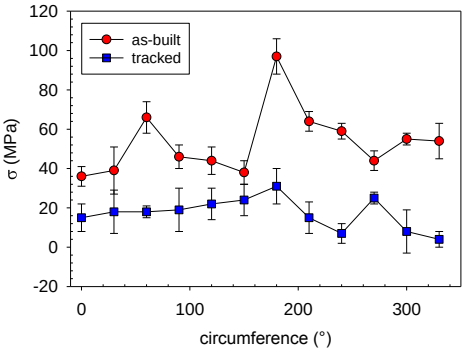

Fig. 4 Comparison of residual stresses of tracked and as-built 40° sample.

The measured data were fitted with the von Mises condition with a yield strength of an average value of 160 MPa (corresponding to 0.005% of plastic strain). The same value was evaluated from a tensile test. The yield strength (corresponding to 0.2% of plastic strain) is given by around 255 MPa. Compared to the maximum value of RS (Fig. 1), which is 100 MPa for the aluminium phase, it is possible to state that in some surface RS reach 63% of the yield strength and, therefore; 60 MPa of external tensile stress will result in plastic deformation. The higher yield strength in compression, which is obvious from Fig. 3, is the confirmation of the tensile residual stress observed by XRD analyses. Nevertheless, the results from Al phase are influenced by both Al, in solid solution and eutectoid too, where one of the Al phase should be harder and, therefore; one Al phase should be in elastic and the second in the plastic region.

Tracking of the yield surface leads to cyclic plastic deformation, which reduces the average crystallite size from values of 122 and 16 nm to 116 and 14 nm for Al and Si phases, respectively. The RS of Al phase were redistributed/reduced and homogenized their values; see Fig. 4.

Conclusion

The slope of the printing (printing strategy) does not affect the phase composition, nevertheless; it affects the values of RS and their inhomogeneities around the circumference of tubular samples. Moreover, all analysed RS were tensile. The difference between the maximum and minimum values around the circumference reaches up to 60 MPa. These inhomogeneities, the so-called surface microstructure notches (step changes in RS and/or microstructure parameters) are prone to fatigue crack formation, which has a major influence on fatigue life.

The worst low-cycle fatigue life was found for the 0° sample (results will be the subject of another article), probably due to the presence of pores in the critical layer parallel to the printing platform. Furthermore, the decrease in fatigue life can be attributed to the stress inhomogeneities of the RS of the 40° sample.

The yield strength of 160 MPa of the 40° sample was determined by tracking. It can be assumed that this value is lower than for conventional-made samples because it is related to the real structure of the SLM printed samples, i.e., the presence of pores, printing layers, etc.

Acknowledgements

Measurements were supported by the project 23-05338S of the Czech Science Foundation. The work of CTU staff was supported by the grant number CZ.02.1.01/0.0/0.0/16_019/0000778 "Center for Advanced Applied Science" within the Operational Program Research, Development and Education supervised by the Ministry of Education, Youth and Sports of the Czech Republic and the Grant Agency of the Czech Technical University in Prague, grant No. SGS22/183/OHK4/3T/14.

References

[1] Bartlett, J.L. and Li, X. "An overview of residual stresses in metal powder bed fusion," *Additive Manufacturing*, **27**, pp. 131-149 (2019).

[2] Schneller, W., Leitner, M., Pomberger, S., Springer, S., Beter, F. and Grün, F. "Effect of post treatment on the microstructure, surface roughness and residual stress regarding the fatigue strength of selectively laser melted AlSi10Mg structures," *Journal of Manufacturing and Materials Processing*, **3**(4), pp. 89 (2019).

[3] Čapek, J., Trojan, K., Kec, J., Černý, I., Ganev, N. and Němeček, S. "On the Weldability of Thick P355NL1 Pressure Vessel Steel Plates Using Laser Welding," *Materials*, **14**(1), pp. 131 (2020).

[4] Černý, I., Čapek, J., Kec, J., Trojan, K., Ganev, N. and Němeček, S. "Fatigue of Laser-Welded Structures: Role of Residual Stress," in *Comprehensive Structural Integrity*, Aliabadi F. and Soboyejo W., ed. (Elsevier Science, 2023), ISBN 9780128229446.

[5] Kraus, I. and Ganev, N. Technické aplikace difrakční analýzy (ČVUT, Praha, 2004).

[6] Štefan, J., Parma, S., Marek, R., Plešek, J., Ciocanel, C. and Feigenbaum, H. "Overview of an Experimental Program for Development of Yield Surfaces Tracing Method," *Applied Sciences*, **11**(16), 7606 (2021).

[7] Gil, C.M., Lissenden, C.J. and Lerch, B. A. "Determination of Yield in Inconel 718 for Axial-Torsional Loading at Temperatures up to 649 C," *NASA/TM*, pp. 1-33 (1998).

[8] ASTM E2207 - 15 Standard Practice for Strain-Controlled Axial-Torsional Fatigue Testing with Thin-Walled Tubular Specimens. West Conshoshocken (USA: ASTM International, 2015).